Rare Metal Materials and Engineering
Volume 51, Issue 3, March 2022
Available online at www.rmme.ac.cn

Science Press

Cite this article as: Yu Zhuhuan, Fei Zhenbao, Yan Yawen, et al. Effect of Solution Heat Treatment on Microstructure and Segregation of Carbon-Containing Nickel-based Single Crystal AM3 Superalloy[J]. Rare Metal Materials and Engineering, 2022, 51(03): 806-813.

ARTICLE

Effect of Solution Heat Treatment on Microstructure and Segregation of Carbon-Containing Nickel-based Single Crystal AM3 Superalloy

Yu Zhuhuan, Fei Zhenbao, Yan Yawen, Qiang Junfeng, Gao Wei, Wang Xiaohui, Liu Xuliang, Yi Dawei

College of Materials Science and Engineering, Xi'an University of Science and Technology, Xi'an 710054, China

Abstract: The effect of different solution treatments on the microstructure and element segregation of AM3 nickel-based single crystal superalloys with the carbon content of 0.045wt% was investigated. The optical microscope (OM) and scanning electron microscope (SEM) were used to observe the microstructure and γ' phase of AM3 superalloys, and the electron-probe microanalysis (EPMA) was used to analyze the element segregation. The results show that the incipient melting temperature of the AM3 superalloys is 1305 °C. After the solution treatment of 1305 °C/6 h following the homogenization treatment of 1300 °C/3 h, the incipient melting structure is reduced, and the incipient melting temperature is increased by about 5 °C. With increasing the solution temperature and prolonging the solution duration, the volume fraction and size of the precipitated γ' phase are increased significantly, and the segregation ratio of Cr, Co, Mo, W, and Al elements is closer to 1. The existence of incipient melting structure prevents the segregation of Ti in AM3 superalloys with prolonging the solution duration after heat treatment. Thus, the optimum heat treatment process is 1300 °C/3 h+1305 °C/6 h/air cooling (AC)+1080 °C/6 h+870 °C/20 h/AC. The dendrite structure of AM3 single crystal superalloys completely disappear after heat treatment. The cubic degree of γ' phase is improved, the size of γ' phase reaches 454 nm, the volume fraction of γ' phase is 66.05vol%, and the segregation of Cr, Co, Mo, W, Al, and Ti elements is significantly reduced.

Key words: Ni-based single crystal superalloy; directional solidification; solution heat treatment; microstructure; element segregation

Nickel-based single crystal superalloys have wide applications in gas-turbine engine due to their high-temperature bearing capacity and superior mechanical properties[1,2]. During the directional solidification, the solute segregation at the solid-liquid interface causes element segregation in the single crystal superalloy inevitably[3,4]. In the dendrite growth, the W, Mo, Cr, and Co elements accumulate at the dendritic core, whereas the Al, Ti, and Ta elements accumulate in the interdendritic area and then become solidified as the γ' phase and eutectic. The γ' phase is an intermetallic compound based on Ni_3Al with a face-centered cubic (fcc)-like structure, and it is the most important strengthening phase in the nickel-based single crystal superalloys[5-7]. The element segregation occurs in the dendrite core and the interdendritic area of as-cast alloys, which causes different morphologies and sizes of γ' phase. The element segregation and structure heterogeneity have a great influence on the mechanical properties of the alloys, especially the creep properties at high temperatures[8-12]. It is obvious that the dendrite and eutectic structures are significantly reduced, and the difference of γ' phase in the dendritic core and in the interdendritic area is reduced after proper heat treatment. Besides, the γ' phase with uniform size and morphology can be precipitated to achieve better high-temperature mechanical properties[13]. The solution heat treatment and aging treatment are included in comprehensive heat treatment for single crystal superalloys, which firstly dissolves the coarse γ' phase and γ/γ' eutectic structure into the matrix to reduce the element

Received date: March 08, 2021
Foundation item: Excellent Young Teachers Research Program of Xi'an University of Science and Technology (2018YQ2-12); Fund of State Key Laboratory of Solidification Processing of NWPU (SKLSP201846); Sponsored by Science and Technology Activities for Overseas Students in Shaanxi (2018047); Natural Science Basic Research Program of Shaanxi (2020JM-516)
Corresponding author: Qiang Junfeng, Ph. D., Associate Professor, College of Materials Science and Engineering, Xi'an University of Science and Technology, Xi'an 710054, P. R. China, Tel: 0086-29-85587373, E-mail: qjfcamel@163.com

segregation, and then is held at or above the solidus temperature, leading to the incipient melting. The existence of the incipient melting structure can achieve the solid solution strengthening and eliminate the residual stress of superalloys[14-17]. The purpose of aging treatment is to adjust the size of the γ' phase to obtain the optimum combination of strength and plasticity[11,18].

The effects of heat treatment process on the microstructure of Ni-based superalloys have been investigated[19-25]. Tang et al[26] studied the solution heat treatment of GTD111 alloy containing 0.09wt% C and 0.01wt% B at different temperatures, and the results indicated that the coarse γ' phase can be effectively dissolved at 1180~1220 °C after solution heat treatment. The size of γ' phase is decreased with increasing the solution temperature during subsequent cooling process. However, the incipient melting of the alloy occurs at 1240 °C after solution heat treatment. Galizoni et al[27] studied the influence of heat treatment on the microstructure of Inconel 713C nickel-based superalloy with 0.14wt% C, 0.01wt% B, and 0.1wt% Zr, and found that the microstructure changes after the heat treatment. $NbNi_3$-rich carbides are formed, which increases the niobium content in the carbides. Zhou et al[28] analyzed the solution heat treatment of IN718 alloy with 0.08wt% C and 0.006wt% B at different temperatures, and found that Laves phases cannot be completely dissolved after solution heat treatment at 980 °C, and the δ phase is formed. However, the Laves phases can be completely dissolved at 1065 °C with the formation of carbides. Kisasoz et al[29] indicated that the chromium-rich $M_{23}C_6$ carbides can be formed after the solution heat treatment at 1040 °C for 1 h for G-NiCr28W alloys. The bulk W-rich Fe_2W_2C carbides can be formed with increasing the solution duration to 8 h. Park et al[30] extended the solution heat treatment duration and found that the refractory elements (Re, W) in the alloys are diffused from the topological close-packed (TCP) phase to the γ' phase, which reduces the precipitation kinetics of TCP phase. Thus, TCP phase in the alloys is decreased or even disappears with prolonging the solution duration. However, Yin et al[31] showed that TCP phase is abnormally increased and more μ phase appears after long-term solution treatment at 900 °C for the nickel-based single crystal superalloys with 0.05wt% C. Cui et al[32] studied the effect of solution heat treatment on the microstructure of DD5 alloys with 3.0wt% Re, 0.15wt% Hf, and 0.05wt% C, and presented that the solution treatment at 1290~1310 °C for 2~6 h has no obvious influence on the microstructure.

Kubin et al[33] studied the effect of standard heat treatment on the mechanical properties of carbon-free AM3 single crystal superalloys, but the heat treatment for carbon-containing nickel-based single crystal AM3 superalloys is rarely investigated. Although the solidification path, solidification structure, and high temperature mechanical properties of carbon-containing single crystal AM3 superalloy have been studied[34-40], the optimum heat treatment process is still unclear. It is necessary to study the solution treatment because it is the premise that the alloy can precipitate more suitable γ' phase during aging treatment.

Therefore, the effect of different heat treatments on the microstructure and element segregation was studied in this research, and it provided a theoretical basis for the development and application of the single crystal superalloys.

1 Experiment

The chemical composition of the nickel-based AM3 superalloys is shown in Table 1. The VDS-1 directional solidification furnace with seed method was used in this research. The preferred [001] direction was within 5° from the longitudinal axis. The cylindrical specimens of 5 mm in height were cut from the single crystal rods for subsequent heat treatment experiments. The solidification was performed at a holding temperature of 1650 °C and a constant withdrawal rate of 50 μm/s.

The heat treatments were performed in SX2-9-17TP type high temperature furnace with the temperature fluctuation of ±1 °C. The γ' phase has the solvus temperature, liquidus temperature, and solidus temperature of 1293.5, 1329.2, and 1361.0 °C, respectively[41]. In this experiment, seven different solution heat treatment processes were designed, as shown in Table 2. All specimens were finally treated by aging process of 1080 °C/6 h+870 °C/20 h/air cooling (AC) to precipitate the γ' phase.

In order to observe the dendrite structure and γ' phase of the alloys, the as-cast alloy and the specimens after heat treatment were ground, polished, and etched by 10 mL HNO_3+20 mL HF+30 mL $C_3H_8O_3$.

The dendrite structure of AM3 superalloys was observed by an OLYMPUS-GX71 optical microscope (OM). The dendrite arm spacings were measured by Image J software. The γ' phase was observed by a S-4800 scanning electron

Table 1 Chemical composition of nickel-based AM3 superalloys (wt%)

C	Cr	Co	Mo	W	Al	Ti	Ta	Ni
0.045	7.82	5.34	2.25	4.88	6.02	1.94	3.49	Bal.

Table 2 Heat treatment processes of nickel-based AM3 superalloys

Specimen	Solution heat treatment	Aging heat treatment
HT1	1305 °C/6 h/AC	1080 °C/6 h +870 °C/20 h/AC
HT2	1305 °C/3 h/AC	
HT3	1310 °C/3 h/AC	
HT4	1295 °C/3 h +1300 °C/6 h/AC	
HT5	1300 °C/3 h +1305 °C/6 h/AC	
HT6	1305 °C/3 h +1310 °C/6 h/AC	
HT7	1285 °C/3h+1290 °C/6 h +1295 °C/9 h/AC	

microscope (SEM). The mean size and the volume fraction of γ' phase were measured by Image J software.

Element segregation was analyzed by JXA8100 electron probe microanalysis (EPMA). It was difficult to specify the dendrite core (DC) and the interdendritic area (IA) due to the elimination of dendrite structure after heat treatment. Thus, In order to study the element segregation of AM3 superalloys after heat treatment, the point scanning matrix technique[42] was used to uniformly distribute 8×8=64 points in an area of 800 μm×800 μm (Fig.1), and the dwelling time was 30 s per point. The EPMA accelerating voltage used for the point scanning matrix technique was 15 kV, and the accelerating current was 21 μA.

The residual segregation ratio k was defined as follows:

$$k=\frac{\left(\sum_{i=1}^{m}k_i^{\mathrm{DC}}\right)/m}{\left(\sum_{i=n-m}^{n}k_i^{\mathrm{IA}}\right)/(n-m)} \quad (1)$$

where m is the total number of points in DC area; n is the total number of measured points; k_i^{DC} and k_i^{IA} are the components of each point in DC and IA, respectively. The content at each point and the average content were used to divide the dataset into DC and IA parts, respectively. The points with greater contents of positive segregation elements (Al, Ti, and Ta) than the average content were considered as IA part, whereas those with smaller contents of positive segregation elements were considered as DC part. The points with greater contents of negative segregation elements (Co and W) than the average content were considered as DC part, while the points with smaller contents of negative segregation elements than the average content were considered as IA part[43]. The measured 64 points were all used to calculate the residual segregation ratio k for accuracy.

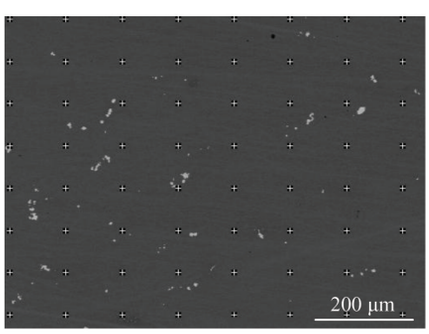

Fig.1 Microscope image for element segregation determination by point scanning matrix technique

2 Results and Discussion

2.1 Microstructure

2.1.1 As-cast AM3 superalloy

Fig.2 shows the morphologies of as-cast single crystal AM3 superalloys along the transverse and longitudinal directions. It can be observed that the as-cast AM3 superalloy exhibits a regularly arranged dendritic structure. DC exhibits cross pattern, and there are many white γ/γ' eutectic structures in IAs. A single-phase solid solution is formed in DC during the solidification process, and Al, Ti, and Ta elements are enriched in IAs. Thus, the solute concentration in the remaining liquid phase reaches the eutectic point, forming γ/γ' eutectic structures. The average primary dendrite arm spacing is 194 μm. Fig.2b shows the quenched morphology of AM3 superalloy with a dendritic growth interface under a withdrawal rate of 50 μm/s. When the alloy solidifies at the dendritic interface, the dendrite substructures are formed in the single crystal structure due to the segregation of solute elements. The average secondary dendrite arm spacing of AM3 superalloy is 482 μm.

2.1.2 Heat-treated AM3 superalloy

Fig.3 shows OM microstructures of AM3 superalloys after different heat treatments. Obviously, the dendritic and the eutectic structures are reduced significantly. According to Fig.3a~3c, it is found that prolongation of solution duration by 3 h causes the incipient melting. The structure of incipient melting consists of re-solidified γ/γ' eutectics and micropores (Fig.3a). With increasing the solution temperature by 5 °C, the incipient melting occurs, and the incipient melting structures are connected (Fig.3c). No incipient melting can be observed in HT2 specimen after heat treatment at solution temperature of 1305 °C for 3 h (Fig.3b). Therefore, the effect of increasing the solution temperature by 5 °C on the microstructure is more serious than that of prolonging the solution time by 3 h. It can be seen that the dendrite structure completely disappears in HT5 specimen without incipient melting (Fig. 3e). The elements are not sufficiently diffused in HT4 specimen, and there is still an ambiguous dendritic structure after the heat

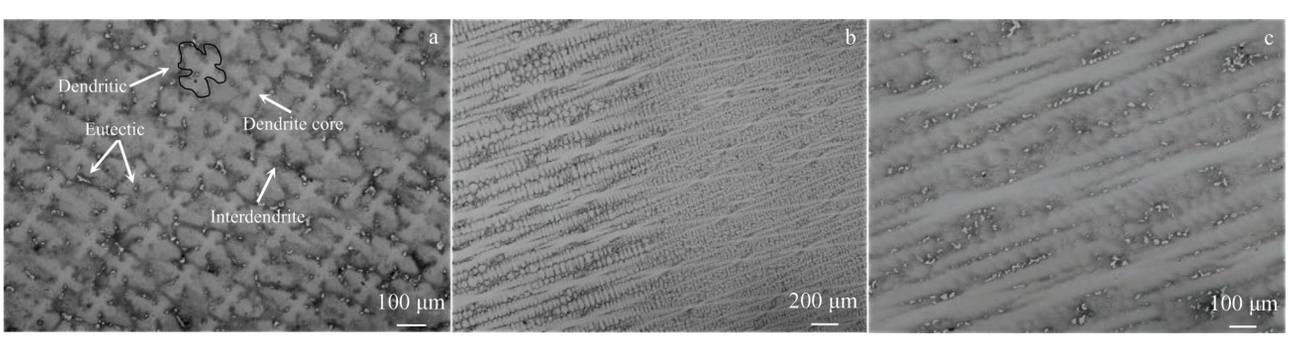

Fig.2 Transverse (a) and longitudinal (b, c) interface morphologies of as-cast AM3 superalloys

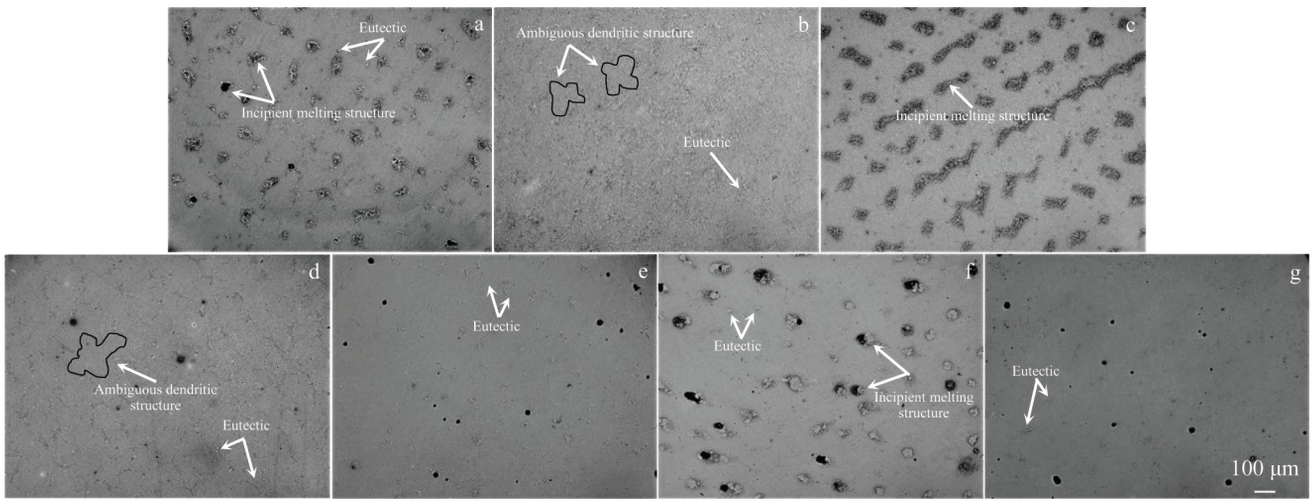

Fig.3 OM microstructures of AM3 superalloy specimens after different heat treatments: (a) HT1, (b) HT2, (c) HT3, (d) HT4, (e) HT5, (f) HT6, and (g) HT7

treatment at solution temperature of 1300 °C (Fig. 3d). The heat treatment of 1305 °C/3 h+1310 °C/6 h/AC does not significantly increase the incipient melting temperature through homogenization, and the essential element diffusion rate is slower than the element diffusion rate caused by the increasing temperature during the solution treatment process, which results in the incipient melting of AM3 superalloys (Fig. 3f). This is because the peak solution temperature is higher than the incipient melting temperature of AM3 superalloys, and the solution treatment duration is shorter. Comparing Fig. 3a with 3e, it can be found that the homogenization treatment at 1300 °C/3 h before solution heat treatment at 1305 °C/6 h leads to more complete diffusion of refractory metal elements. Therefore, the incipient melting temperature of γ substrate is increased but within 5 °C due to the shorter homogenization duration. It is also noted that the homogenization treatment reduces the volume fraction of the incipient melting structure. The comparison between Fig. 3b with 3f shows that increasing the solution temperature and prolonging the solution duration result in significant incipient melting for AM3 superalloys still with dendrites. By comparing Fig. 3d with 3g, it can be found that with further prolonging the solution duration and decreasing the solution temperature, AM3 superalloy does not undergo the initial melting, and the dendrite structure completely disappears. According to the microstructure analysis of AM3 superalloy after different heat treatments, it is concluded that the HT5 and HT7 specimens have improved microstructures, i.e., the heat treatments of 1300 °C/3 h+1305 °C/6 h/AC and 1285 °C/3 h+1290 °C/6 h+1295 °C/9 h/AC are better in comprehensive consideration.

2.2 γ' phase

It is well known that the γ matrix has fcc structure and the γ' phase has fcc-like structure. Their lattice mismatch is very small and the solute supersaturation is high, which is conducive to the nucleation of the γ' phase from γ supersaturated solid solution[44]. Fig. 4 shows the changed morphologies of γ' phase after casting and different heat treatments. The γ matrix of white grid is separated by the large black γ' phase. It can be seen from Fig. 4a that the as-cast γ' phase is butterfly-shaped and irregular. The arrangement and distribution of γ' phase are not uniform. Fig. 4b~4h indicate that the γ' phase has the cube and strip shape after heat treatment. The arrangement and distribution of γ' phase are more uniform due to the solution treatment through element diffusion. With increasing the solution temperature and prolonging the solution duration, the element diffusion is more sufficient. The γ/γ' eutectic structure and the coarse γ' phase formed during the solidification process can be fully solid-dissolved in the γ matrix, which achieves the homogenization structure. Therefore, the γ' phase with a more uniform size and distribution is precipitated in the subsequent cooling process. As shown in Fig. 4b~4g, the morphologies of regularly arranged cube of γ' phase do not change in HT1~HT6 specimens. However, there is a tiny radian at the apex angles of the γ' phase in Fig. 4h.

Fig. 5 shows the size of γ' phase of AM3 superalloys after casting and different heat treatments. It can be seen that the size of γ' phase in AM3 superalloys after heat treatment is obviously larger than that in as-cast AM3 superalloys. The size of γ' phase of HT1 and HT3 specimens is larger than that in HT2 specimen, because the increased solution temperature accelerates the decrease in interfacial energy and promotes the element diffusion caused by the γ' phase, which results in increasing annexation and growth of γ' phases. Similarly, prolonging the solution duration also causes the γ' phase occurrence and growth. Eventually, the size of γ' phase is increased. The size of γ' phase in HT3 specimen is larger than that in HT1 specimen, indicating that the effect of increasing the solution temperature on the γ' phase size is more obvious than that of prolonging the solution duration. For HT4, HT5, and HT6 specimens, it can be seen that with increasing the

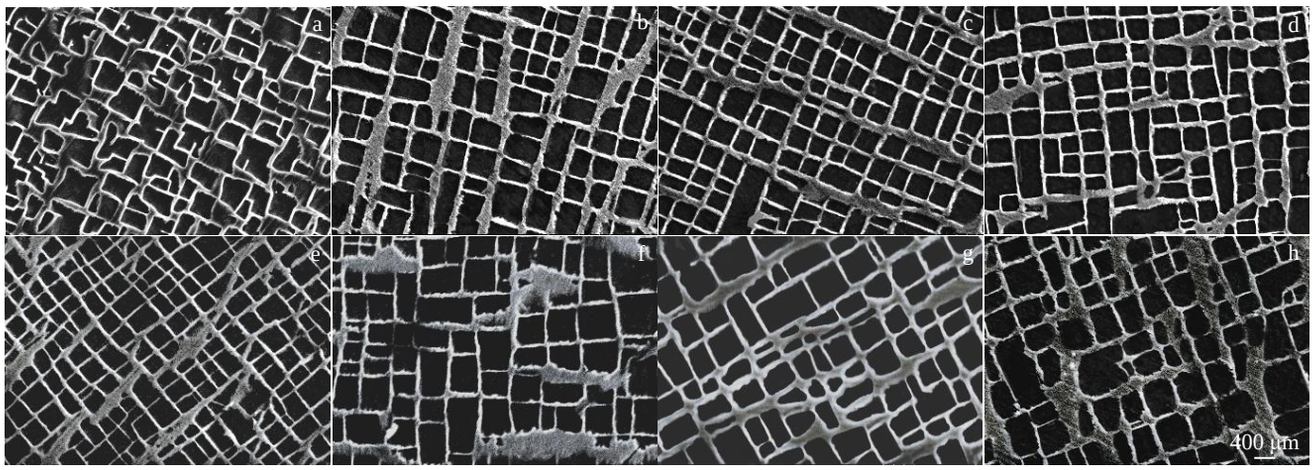

Fig.4 Microstructures of γ' phase after casting (a) and different heat treatments (b~h): (b) HT1, (c) HT2, (d) HT3, (e) HT4, (f) HT5, (g) HT6, and (h) HT7

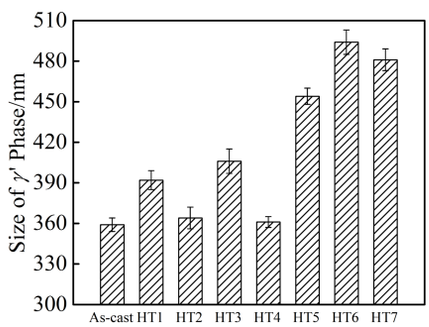

Fig.5 Size of γ' phase in AM3 superalloys after casting and different heat treatments

solution temperature, the size of the γ' phase is gradually increased. The size of γ' phase in HT5 and HT6 specimens is 454 and 494 nm, respectively. For HT7 specimen, the effect of solution temperature is partially offset due to the longer solution duration. When the peak temperature is 1295 °C, the size of the γ' phase in HT7 specimen reaches 481 nm.

Fig. 6 shows the volume fraction of γ' phase of AM3 superalloys after casting and different heat treatments. It can be seen that the volume fraction of γ' phase in AM3 superalloys after heat treatment is obviously larger than that in

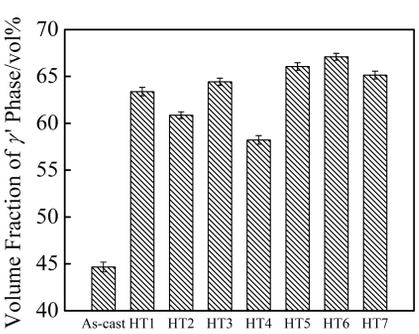

Fig.6 Volume fraction of γ' phase in AM3 superalloys after casting and different heat treatments

as-cast AM3 superalloys. The volume fraction of γ' phase in HT1 and HT3 specimens is significantly larger than that in HT2 specimen. For HT4, HT5, and HT6 specimens, it can be seen that the volume fraction of γ' phase is increased significantly with increasing the solution temperature. The volume fraction of γ' phase in HT5 and HT6 specimens reaches 66.05vol% and 67.09vol% , respectively, which is larger than that in HT7 specimen. There is sufficient time for γ' phase to grow in HT7 specimen due to the further prolonged solution duration by 9 h, and therefore the volume fraction of γ' phase in HT7 specimen (65.14vol%) is larger than that in HT4 specimen. The coarse γ' phase in the as-cast specimen can be completely dissolved in the matrix with increasing the solution temperature and prolonging the solution duration. During the subsequent cooling process, the volume fraction of the precipitated γ' phase is increased significantly.

The high temperature rupture property of nickel-based single crystal AM3 superalloys is related to the shape, volume fraction, and size of the γ' phase. The good cubic degree and large volume fraction of γ' phase both contribute to the improvement in alloy properties. The effect of γ' phase size on the properties is particularly important due to the interaction between the γ' phase and dislocations. Under the high temperature and low stress, the dislocations bypass the γ' phase. When the γ' phase size is large, the path of the dislocations to bypass the γ' phase will be extended. Besides, the regular γ' phase is conducive to the rapid formation of raft structure. These are all enhancement mechanisms for the high temperature rupture property of alloys. However, when the heat treatment temperature is too high, the raft thickness of γ' phase is overly increased, which is disadvantageous for the high temperature rupture property of alloys. Therefore, it is extremely important to form a γ' phase with an appropriate size. Ref. [45-47] reported that the high temperature rupture creep property achieves the optimum state for the first generation of superalloys, when the γ' phase is cubic and regularly arranged with a phase size of 450 nm and a volume fraction of about 65%. After the comprehensive analysis, it

can be concluded that the heat treatment of 1300 °C/3 h+1305 °C/6 h/AC can optimally improve the mechanical properties of AM3 superalloys.

2.3 Element segregation

The degree of element segregation under different heat treatments is shown in Fig.7 and Fig.8. It can be seen that the degree of Mo segregation is the most serious, and that of Cr segregation is the least serious. The degree of segregation for Cr, Co, Mo, and W elements becomes more serious in HT4 and HT2 specimens due to the presence of residual dendrite structure. The degree of segregation of Mo and W in HT4 specimen is more serious than that in HT2 specimen, and there is no significant difference in the degree of segregation of Cr and Co. Thus, the increase in solution temperature is more conducive to the reduced degree of segregation for Mo and W. The segregation of Cr, Co, Mo, and W is reduced in HT7 specimen, compared with that in HT2 specimen. Therefore, the peak solution temperature of 1305 °C and the improved element diffusion both lead to the fact that the segregation ratio of Cr, Co, Mo, and W elements is larger but closer to 1 with prolonging the solution duration.

Fig. 8 shows the positive segregation ratio of AM3 superalloys after different heat treatments. Similarly, the segregation of Al and Ti is more severe due to the presence of residual dendrite structure in HT4 and HT2 specimens, and the segregation of Ti is more serious than that of Al. In addition, the degree of segregation of Al and Ti in HT7 specimen is smaller than that in HT2 specimen, because the dendrite structure is completely eliminated in HT7 specimen, presenting a more uniform element distribution. Thus, at the solution temperature of 1305 °C, the segregation ratio of Al and Ti is smaller but closer to 1 with prolonging the solution duration. However, it is notable that the degree of segregation of Ti in HT1 specimen is more serious, because the incipient melting occurs in HT1 specimen, and the main element of the incipient melting structure is Ti[48], which causes the enrichment of Ti element. In conclusion, the element segregation is optimally ameliorated in HT5 specimen. The existence of incipient melting structure prevents the segregation ratio of Ti in the alloy from changing regularly with prolonging the solution duration.

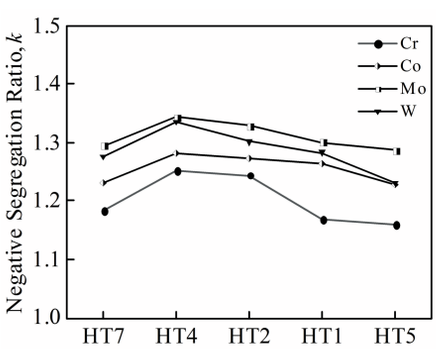

Fig.7 Negative segregation ratio k of AM3 superalloys after different heat treatments

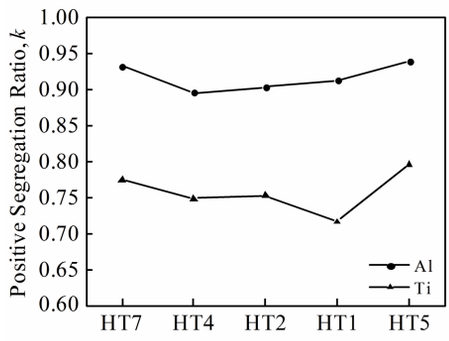

Fig.8 Positive segregation ratio k of AM3 superalloys after different heat treatments

The solution temperature is the most important factor for the element diffusion rate. The higher the solution temperature, the larger the thermal activation energy of the atoms and the faster the atom migration. Eq. (2) shows the Arrhenius equation[49], as follows:

$$D = D_0 \exp\left(-\frac{Q}{RT} \right) \tag{2}$$

where D is the diffusion coefficient, D_0 is the diffusion constant, Q is the diffusion activation energy per mole atom, R is a gas constant of 8.314 $J \cdot mol^{-1} \cdot K^{-1}$, and T is the solution temperature. The values of D_0 and Q are independent of temperature, which are only related to the diffusion mechanism and material. According to the Arrhenius equation, the larger the solution temperature T, the larger the value of D, i. e., with increasing the solution temperature, the diffusion coefficient is larger, the diffusion rate is faster, the diffusion is more sufficient, and element segregation is less.

In addition, the solution duration is also an important influence factor. The degree of element segregation is analyzed by the homogenization kinetic equation or the residual segregation coefficient (δ)[50], as follows:

$$\delta = \frac{C_M^t - C_m^t}{C_M^0 - C_m^0} \tag{3}$$

where C_M^t and C_m^t are the highest and lowest concentrations of elements after the solution for t h, respectively; C_M^0 and C_m^0 are the highest and lowest concentrations in the initial state, respectively. Ref. [51] reported that Eq. (4) is commonly used to represent the change of segregation element concentration with time and location at a certain temperature in the element homogenization process, as follows:

$$C(x) = \bar{C} + \frac{\lambda}{2} \Delta C_0 \cos\frac{2\pi x}{\lambda} \exp\left(-\frac{4\pi^2}{\lambda^2} Dt \right) \tag{4}$$

where $C(x)$ represents the element concentration at the position of x (x=0~λ); C is the average concentration; λ is the dendrite arm spacing; ΔC_0 is the difference between the highest/lowest concentration and the average concentration; t is the solution duration. Therefore, the residual segregation coefficient δ can be obtained by Eq.(5), as follows:

$$\delta = \exp\left(-\frac{4\pi^2}{\lambda^2} Dt \right) \tag{5}$$

It can be seen that the diffusion coefficient and the distance

in IAs are constant. Thus, the longer the solution duration, the smaller the residual segregation δ and the better the solution effect of the alloys.

3 Conclusions

1) The dendrite structures of single crystal AM3 superalloys with 0.045wt% carbon are significantly reduced or even disappear after heat treatment, and the eutectic structures are significantly reduced. The AM3 superalloys undergo three processes with increasing the solution temperature: the dendritic structures are not completely eliminated→the dendritic structures are completely eliminated without incipient melting→the incipient melting occurs. The incipient melting temperature of the alloy is 1305 °C. The homogenization treatment of 1300 °C/3 h before the heat treatment of 1305 °C/6 h reduces the volume fraction of the incipient melting structure, and the incipient melting temperature is increased by 5 °C.

2) The γ' phase shows an irregular butterfly shape with uneven arrangement and distribution in the as-cast AM3 superalloys, whereas that shows the cubic and stripe shape with more uniform arrangement and distribution in AM3 superalloys after heat treatment. The size and volume fraction of γ' phase in alloys after heat treatment are significantly increased. With increasing the solution temperature and prolonging the solution duration, the coarse γ' phase is fully dissolved in the matrix, and the volume fraction and size of the precipitated γ' phase are increased significantly during the subsequent cooling process.

3) The segregation ratio of Cr, Co, Mo, and W is greater than 1, and that of Al and Ti is less than 1 of AM3 superalloys after heat treatment. With increasing the solution temperature and prolonging the solution duration, the segregation ratio of Cr, Co, Mo, W, and Al is closer to 1, and the element diffusion becomes more sufficient. The existence of incipient melting structure prevents the segregation ratio of Ti in the alloy from changing regularly with prolonging the solution duration.

4) The optimum heat treatment for AM3 superalloy is 1300 °C/3 h+1305 °C/6 h/air cooling (AC)+1080 °C/6 h+870 °C/20 h/AC. The dendrite structures are completely eliminated, and no incipient melting occurs. The γ' phase of 454 nm in size and 66.05vol% in volume fraction has a better cubic degree with a uniform arrangement and distribution. The degree of segregation of Al, Ti, Cr, Co, Mo, and W is significantly reduced.

References

1 Ali M A, Galilea I L, Gao S *et al*. *Materialia*[J], 2020, 12: 100 692

2 Utada S, Rame J, Hamadi S *et al*. *Materials Science and Engineering A*[J], 2020, 789: 139 571

3 Yu Z H, Liu B L, Zhai X W *et al. Materials Research Express*[J], 2019, 6(11): 116 544

4 Reinhart G, Grange D, Khalil L A *et al. Acta Materialia*[J], 2020, 194: 68

5 Hu Y L, Lin X, Li Y L *et al*. *Journal of Alloys and Compounds* [J], 2019, 800: 163

6 Xia P C, Xie K, Cui H Z *et al. High Temperature Materials and Processes*[J], 2018, 37(3): 271

7 Zhang Weiguo, Liu Lin, Huang Taiwen *et al. Acta Metallurgica Sinica*[J], 2009, 45(5): 592 (in Chinese)

8 Min Zhixian, Shen Jun, Xiong Yilong *et al. Acta Metallurgica Sinica*[J], 2011, 47(4): 397 (in Chinese)

9 Xia W S, Zhao X B, Yue L *et al. Journal of Materials Science and Technology*[J], 2020, 44(9): 76

10 Xia W S, Zhao X B, Yue L *et al. Journal of Alloys and Compounds*[J], 2020, 819: 152 954

11 Azadi M, Marbout A, Safarloo S *et al. Materials Science and Engineering A*[J], 2018, 711: 195

12 Yu H, Xu W, Zwaag S V D. *Journal of Materials Science and Technology*[J], 2020, 45(10): 207

13 Yu Z H, Qiang J F, Zhang J *et al. Journal of Materials Research* [J], 2015, 30(13): 2064

14 Hegde S R, Kearsey R M, Beddoes J. *Superalloys 2008*[C]. Champion: The Minerals, Metals and Materials Society, 2008: 301

15 Hegde S R, Kearsey R M, Beddoes J C. *Materials Science and Engineering A*[J], 2010, 527(21): 5528

16 Ormastroni L M B, Suave L M, Cervellon A *et al. International Journal of Fatigue*[J], 2020, 130: 105 247

17 Rzyankina E, Pytel M, Mahomed N *et al. International Conference on Competitive Manufacturing*[C]. Stellenbosch: COMA, 2016: 307

18 Kim H T, Chun S S, Yao X X *et al. Journal of Materials Science* [J], 1997, 32(18): 4917

19 Su X L, Xu Q Y, Wang R N *et al. Materials and Design*[J], 2018, 141: 296

20 Condruz M R, Matache G, Paraschiv A *et al. Journal of Thermal Analysis and Calorimetry*[J], 2018, 134(1): 443

21 Wu H Y, Zhuang X L, Nie Y *et al. Materials Science and Engineering A*[J], 2019, 754: 29

22 Meid C, Dennstedt A, Ramsperger M *et al. Scripta Metallurgica* [J], 2019, 168: 124

23 Huang Y S, Wang X G, Cui C Y *et al. Materials Science and Engineering A*[J], 2020, 773: 138 886

24 Wang Tao, Wan Zhipeng, Li Zhao *et al. Acta Metallurgica Sinica* [J], 2020, 56(2): 182 (in Chinese)

25 Zhang Y B, Liu L, Huang T W *et al. Scripta Metallurgica*[J], 2017, 136: 74

26 Tang Wenshu, Xiao Junfeng, Li Yongjun *et al. Acta Metallurgica Sinica*[J], 2019, 55(5): 601 (in Chinese)

27 Galizoni B B, Couto A A, Reis D A P. *Metals*[J], 2019, 9(1): 10

28 Zhou L, Mehta A, McWilliams B *et al. Journal of Materials Science and Technology*[J], 2019, 35(6): 1153

29 Kisasoz A. *China Foundry*[J], 2019, 16(1): 63

30 Park K H, Withey P. *Advanced Engineering Materials*[J], 2018, 20(7): 1 700 987
31 Yin B, Xie G, Lou L H *et al. Scripta Materialia*[J], 2019, 173: 1
32 Cui Renjie, Huang Zhaohui, Guan Kai *et al. Transactions of Materials and Heat Treatment*[J], 2019, 40(6): 45 (in Chinese)
33 Kubin L P, Lisiecki B, Caron P. *Philosophical Magazine A*[J], 1995, 71(5), 991
34 Yu Z H, Liu L, Zhang J. *Transactions of Nonferrous Metals Society of China*[J], 2014, 24(2): 339
35 Yu Z H, Liu L, Zhao X B *et al. Rare Metal Materials and Engineering*[J], 2011, 40(8): 1407 (in Chinese)
36 Zhao X B, Liu L, Yu Z H *et al. Journal of Materials Science*[J], 2010, 45(22): 6101
37 Yang C B, Liu L, Zhao X B *et al. Applied Physics A*[J], 2014, 114(3): 979
38 Yu Z H, Liu L, Zhao X B *et al. Transactions of Nonferrous Metals Society of China*[J], 2010, 20(10): 1835
39 Yu Zhuhuan, Liu Lin. *Acta Metallurgica Sinica*[J], 2014, 50(7): 854 (in Chinese)
40 Zhao Xinbao, Liu Lin, Zhang Weiguo *et al. Rare Metal Materials and Engineering*[J], 2011, 40(1): 9 (in Chinese)
41 Yu Zhuhuan. *Effect of Carbon Addition on the Solidification Microstructure and Mechanical Properties of Single Crystal Superalloys*[D]. Xi'an: Northwestern Polytechnical University, 2011 (in Chinese)
42 Liu Gang, Han Zhenhua, Yang Xin. *Hot Working Technology*[J], 2018, 47(21): 93 (in Chinese)
43 Paraschiv A, Matache G, Puscasu C. *Transportation Research Procedia*[J], 2018, 29: 303
44 Barjesteh M M, Abbasi S M, Madar K Z *et al. Materials Chemistry and Physics*[J], 2019, 227: 46
45 Caron P, Khan T. *Aerospace Science and Technology*[J], 1999, 3(8): 513
46 Caron P, Khan T. *Materials Science and Engineering*[J], 1983, 61(2): 173
47 Steuer S, Hervier Z, Thabart S *et al. Materials Science and Engineering A*[J], 2014, 601: 145
48 Ning Likui, Zheng Zhi, Jin Tao *et al. Acta Metallurgica Sinica* [J], 2014, 50(8): 1011 (in Chinese)
49 Hu Gengxiang. *Fundamentals of Materials Science*[M]. Shanghai: Shanghai Jiaotong University Press, 2010 (in Chinese)
50 Karunaratne M S A, Cox D C, Carte P et al. *Superalloys 2000* [C]. Champion: The Minerals, Metals and Materials Society, 2000: 263
51 Zhu Guanni, Bi Zhongnan, Dong Jianxin *et al. Chinese Journal of Engineering*[J], 2010, 32(5): 628 (in Chinese)

固溶热处理对含碳镍基单晶高温合金AM3组织和偏析的影响

余竹焕，费祯宝，阎亚雯，强军锋，高　炜，王晓慧，刘旭亮，易大伟
(西安科技大学 材料科学与工程学院，陕西 西安 710054)

摘　要：研究了不同固溶处理工艺对含0.045%（质量分数）碳的AM3镍基高温合金组织和元素偏析的影响。采用光学显微镜和扫描电镜对组织和γ′相进行了观察分析。采用电子探针对元素偏析进行了测试分析。结果显示，合金的初熔温度为1305 ℃，在对试样进行1305 ℃/6 h固溶处理前，对其先进行1300 ℃/3 h的均匀化处理可以减少初熔组织的出现，并能使得初熔温度提高约5 ℃。随着固溶温度的提高和固溶时间的延长，γ′相的体积分数和尺寸显著增大，元素Cr、Co、Mo、W和Al的偏析系数接近均值1。随着固溶时间的延长，初熔组织的出现阻碍了Ti的偏析。最佳的固溶处理工艺为1300 ℃/3 h+1305 ℃/6 h/空冷+1080 ℃/6 h+870 ℃/20 h/空冷。热处理后的AM3单晶高温合金枝晶组织完全消失，γ′相立方度更好，尺寸达到454 nm，并且体积分数为66.05%。元素Cr、Co、Mo、W、Al和Ti的偏析程度均有所降低。

关键词：镍基单晶高温合金；定向凝固；固溶热处理；微观结构；元素偏析

作者简介：余竹焕，女，1978年生，博士，副教授，西安科技大学材料科学与工程学院，陕西 西安 710054，电话：029-85587373，E-mail：yzh0709qyy@xust.edu.cn